

Article

Not peer-reviewed version

INterpolated FLOod Surface (INFLOS), a Rapid and Operational Tool to Estimate Flood Depths from Earth Observation Data for Emergency Management

Alessandro Caretto , [Quentin Poterek](#) , Rémi Braun , [Stephen Clandillon](#) ^{*} , Claire Huber , [Pietro Ceccato](#)

Posted Date: 12 August 2024

doi: 10.20944/preprints202408.0739.v1

Keywords: flood depth; interpolation; digital terrain model; remote sensing; emergency management



Preprints.org is a free multidiscipline platform providing preprint service that is dedicated to making early versions of research outputs permanently available and citable. Preprints posted at Preprints.org appear in Web of Science, Crossref, Google Scholar, Scilit, Europe PMC.

Copyright: This is an open access article distributed under the Creative Commons Attribution License which permits unrestricted use, distribution, and reproduction in any medium, provided the original work is properly cited.

Article

INterpolated FLOod Surface (INFLOS), a Rapid and Operational Tool to Estimate Flood Depths from Earth Observation Data for Emergency Management

Alessandro Caretto¹ , Quentin Poterek¹ , Rémi Braun¹ , Stephen Clandillon^{1,*} , Claire Huber¹ and Pietro Ceccato² 

¹ ICube-SERTIT, University of Strasbourg, 300 Bd Sébastien Brant, 67 412 Illkirch-Graffenstaden, France; acarotto@unistra.fr, q.poterek@unistra.fr, remi.braun@unistra.fr, s.clandillon@unistra.fr, claire.huber@unistra.fr

² DG-Joint Research Centre, Via Enrico Fermi 2749, I-21 027 Ispra (VA), Italy; pietro.ceccato@ec.europa.eu

* Correspondence: s.clandillon@unistra.fr

Abstract: The Rapid Mapping (RM) component of the Copernicus Emergency Management Service (CEMS) delivers crisis information within hours or days, during and in the immediate aftermath of a disaster. Users of the service have requested the incorporation of flood depth estimates for inundations and related disasters, such as storms and tsunamis. This demand required the development of a quick and operational approach for estimating floodwater depth distribution, which can effectively adapt to a wide range of flood scenarios, remotely sensed data and Digital Terrain Models (DTMs). INFLOS is a tool developed to answer these requirements, within an expedient 30-minute timeframe at most. It uses sample points collected along the edges of flooded areas derived from remotely sensed imagery, and integrates high resolution DTMs and hydrography data to enhance accuracy. Flood depth is then estimated through a multi-step interpolation and filtering process. INFLOS underwent thorough testing across fourteen regions. As it transitioned into production, INFLOS successfully generated a wealth of flood depth products accessible through the CEMS RM portal: <https://emergency.copernicus.eu/mapping/list-of-activations-rapid>. Currently, INFLOS is operational and its computation time remains consistently within the order of minutes, making it a staple of the RM tooling and portfolio.

Keywords: flood depth; interpolation; digital terrain model; remote sensing; emergency management

1. Introduction

1.1. Context

Floods are among the most destructive natural disasters worldwide, affecting millions of people and causing significant economic and environmental damage. Climate change and its complex feedback mechanisms have made monitoring the hydrological cycle, including flood events, increasingly challenging. Research indicates that precipitation patterns, flood frequency, and intensity are experiencing anomalies [1], with a notable increase in reported floods since 1950, according to the EM-DAT repository [2] as illustrated in Figure 1. Moreover, flood-related events account for more than 33% of all reported disasters in 2023. This surge highlights the inadequacy of current flood prevention, management, and monitoring systems, owing to the erratic and changing climate and weather patterns [3].

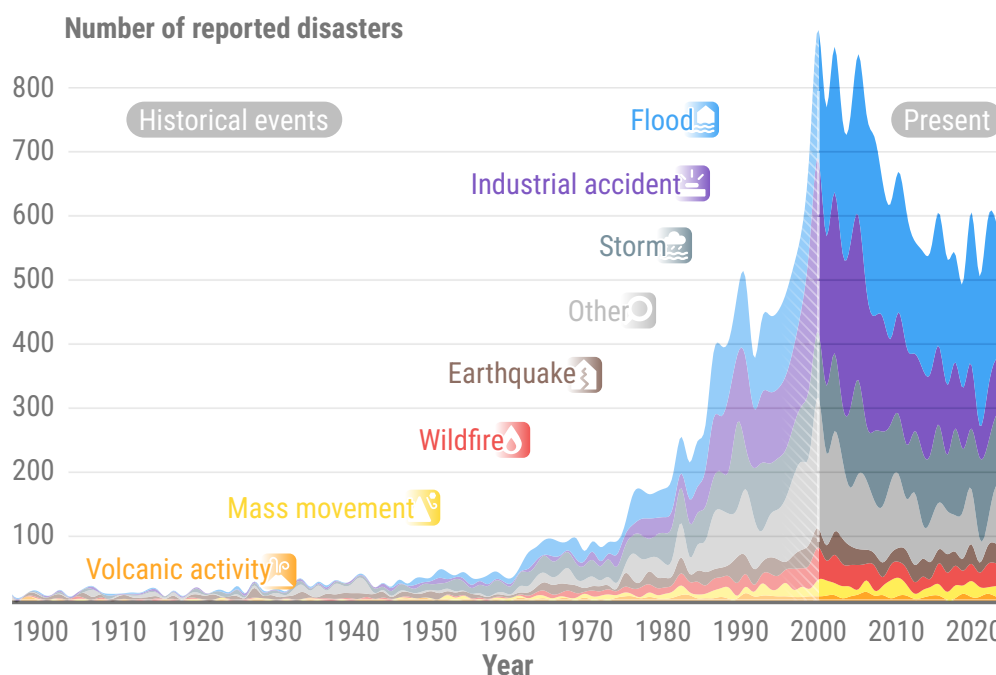


Figure 1. Number of reported natural and technological disasters, between 1900 and 2023, according to EM-DAT [2]. The EM-DAT classification scheme was changed to better align with CEMS RM main disaster classes. Historical events, prior to 2000, are subject to biases. Year 2024 is omitted, for data validation is still pending.

As a result, approximately 1.47 billion people worldwide face a high risk of severe flooding [4]. Urban areas pose a significant concern, due to their high population density and proximity to large watercourses and coastlines, resulting from economic drivers [5]. In Europe, for example, 51% of the population lives in coastal regions [6], and the median distance between people and the nearest water body is 3 kilometres [7]. This emphasises the need for robust flood management strategies to protect these densely populated areas. The rapid pace of urbanisation, which is expected to add 2.5 billion people to urban centres by 2050 [8], will further exacerbate flood risks.

As urban expansion continues, it is essential for policymakers, urban planners, and civil security services to have access to reliable data to support flood management, mitigation efforts and recovery strategies. Traditional monitoring methods, such as ground-based surveys and aerial photography, provide precise information, but may not offer real-time data during crises. Remotely sensed satellite imagery and advanced computer vision techniques offer a more efficient, timely and comprehensive solution for flood monitoring and damage assessment [9]. This approach has become the leading solution for crisis data collection and provision, especially due to the increased frequency of major disasters [10]. The growing availability of high-resolution satellite images has significantly improved the accuracy and timeliness of flood mapping. Typical workflows include the use of optical imagery and Synthetic Aperture Radar (SAR) [11]. Optical sensors capture images in the visible and infrared spectra, which can help identify water bodies, flood traces, mudflows and other flood-related features. However, their effectiveness may be limited by the time of acquisition and atmospheric conditions. On the other hand, SAR systems use microwaves that can penetrate clouds and capture data both day and night. This makes them particularly valuable for mapping flood extents, especially during high-precipitation events with dense cloud cover.

Numerous global services utilise remotely sensed data to provide information on floods and their impact, including the Copernicus Emergency Management Service (CEMS), an integral component of the European Union's Copernicus Programme. CEMS is dedicated to delivering timely and accurate geospatial information to support disaster management and civil protection authorities globally.

Authorized users, such as national civil protection authorities, European Commission services, and the European External Action Service, can access crisis information by triggering the service. CEMS operates 24/7/365, with the Rapid Mapping (RM) framework serving as its core. This framework delivers geospatial information within hours or days following a disaster [12], for various events, including floods, wildfires, earthquakes, and landslides. Examples of provided information include delineation maps that outline the geographical extent of a disaster, and grading maps that assess the impact on populations and assets, such as buildings or transportation networks. From satellite imagery reception to crisis product delivery, operators have up to 7 and 10 hours respectively, for delineation and grading product delivery, highlighting the importance of efficient and reliable workflows.

More specifically, floods and related events, such as tsunamis, storms and mudflows depending on the context, are the most common disasters for which CEMS is activated, accounting for over 46% of the total (Figure 2). CEMS RM users, including EU Directorate Generals and Member State Civil Protection agencies, have requested information on flood depths to enhance emergency relief and impact assessment. This demand requires the development of a rapid and operational methodology that can adapt to various scenarios and integrate into CEMS RM tools. Furthermore, the methodology must be compatible with flood extents derived from different satellite sources, including High Resolution (HR), and Very High Resolution (VHR) imagery, as well as optical and radar sensors.

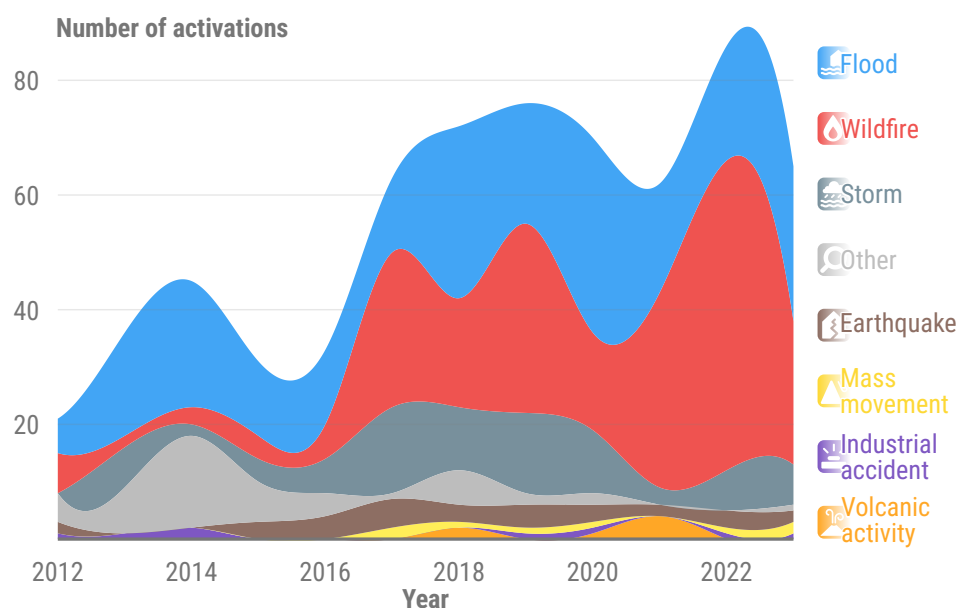


Figure 2. Number of Copernicus Emergency Management Service - Rapid Mapping activations between 2012 and 2023. When applicable, flood activations may also include tsunamis, storms and mudflows, depending on the context of a given event.

1.2. State of the Art

Several methodologies have been developed to estimate flood depth. The most common techniques involve hydrological and hydraulic modelling. These models integrate various inputs, such as meteorological data, land use information, and elevation, to simulate water flow and forecast flood behaviour. However, before integrating these inputs into a modelling solution, several pre-processing steps are required. Furthermore, benchmarks of solutions like HEC-RAS [13], LISFLOOD-FP [14] or FLO-2d [15] suggest simulations that can last for several hours, contingent upon the anticipated precision and spatial resolution relevant for CEMS RM activities [16]. This is particularly true for VHR elevation data, crucial in the context of urban flood mapping [17].

Techniques such as cellular automata (CA) can simplify the physical principles of these models by employing rulesets that describe the behaviour of floodwater in a discrete space, based on topography,

adjacent water cells and other ancillary data if required. This simplification allows CA-based solutions, such as CA-ffé, to run up to 95% faster than conventional methods like HEC-RAS, while producing comparable flood depth results to hydraulic modelling [18]. Further optimisations, such as parallelisation, GPU computing, or memorisation, can further reduce computation times [19] as demonstrated by CADDIES [20]. However, a limitation of CA in rapid mapping is the requirement of an initial state, such as a water volume distribution across the Area Of Interest (AOI), flow rate, or rain gauge readings [21]. These data can be challenging for operators to acquire, given their time constraints and the need for knowledge of local platforms for accessing such information. Typically, CEMS users provide these data when available during an activation, without any guarantee of delivery time, data quality, or compatibility with the CA-based model's expected input.

Alternatively, machine learning-based techniques demonstrate promising results, characterised by rapid inference times and minimal ancillary data or initial state requirements [22]. These methods primarily rely on the flood extent extracted from remotely sensed imagery and a Digital Terrain Model (DTM) from which various topographic indexes can be derived [23]. However, feature engineering can become time-consuming, depending on AOI size, DTM resolution, and necessary topographic information. Moreover, these models require an extensive training dataset and are susceptible to overfitting, among other drawbacks [24], which can lead to inaccurate flood depth patterns.

To reduce the requirement for large computational resources and ancillary data, techniques have been developed that rely solely on remotely sensed information and DTMs to estimate water depths across various flood scenarios [25,26]. FwDET [27] is an example of such a method, which utilises flood polygons to extract elevations from a DTM along the flood boundary. After filtering out samples based on terrain slope, this information is propagated across the flood area using the Nearest Neighbour Interpolation technique to compute floodwater elevations. The final flood depth is determined by subtracting the flood elevation from the DTM. This tool has applications in both riverine and coastal flooding, with the updated FwDET v2.0 addressing coastal complexities and improving computational efficiency [28]. FwDET is widely used in emergency response and disaster resilience research, providing generally accurate and timely flood management support. Although the underlying strategy is promising, testing in the context of CEMS RM activations has proven unsuccessful. Firstly, the iterative Nearest Neighbour interpolation of elevations results in tessellated artefacts, leading to a discrete spatial distribution of depth values despite using a low-pass filter to smooth the associated flood surface. Moreover, sample refinement with terrain slope is insufficient to account for artefacts in the DTMs and their variability, which has proven to be a recurrent issue in an operational setting.

Considering this context, the Interpolated FLOod Surface (INFLOS) tool was developed to fulfil CEMS RM requirements. It utilises an existing flood extent polygon layer derived from remotely sensed imagery combined with the best available DTM. To ensure consistency and robustness across a wide range of applications, several key steps have been implemented, taking reference data and topographic context into consideration. As a result, the proposed approach was operationally tested on more than 180 products worldwide. This paper aims at illustrating the different steps involved in rapidly estimating flood depths from satellite imagery and elevation data, and provides key considerations for both operators and stakeholders when using the generated products.

2. Materials and Methods

INFLOS integrates reference and crisis information gathered, processed, or generated by operators during CEMS RM activations for floods and associated events. The main dependencies of the proposed methodology include data on flooded areas, hydrography, and elevation, as illustrated in Figure 3. Reference information describes the baseline, pre-event conditions, encompassing hydrography and elevation data. Crisis information refers to dynamic data that specifically characterise changes induced by the event, such as newly formed or expanded water bodies. This category also includes any updates to hydrographic features and alterations in terrain or assets caused by the event. The crisis information

is obtained through the analysis of Synthetic Aperture Radar (SAR) images—including Sentinel 1, COSMO-SkyMed, PAZ, RADARSAT-2—, optical images—including Pléiades, Pléiades Neo, GeoEye, WorldView-2, Sentinel-2—or aerial photographs, supported by remote sensing software and libraries such as eoreader [29].

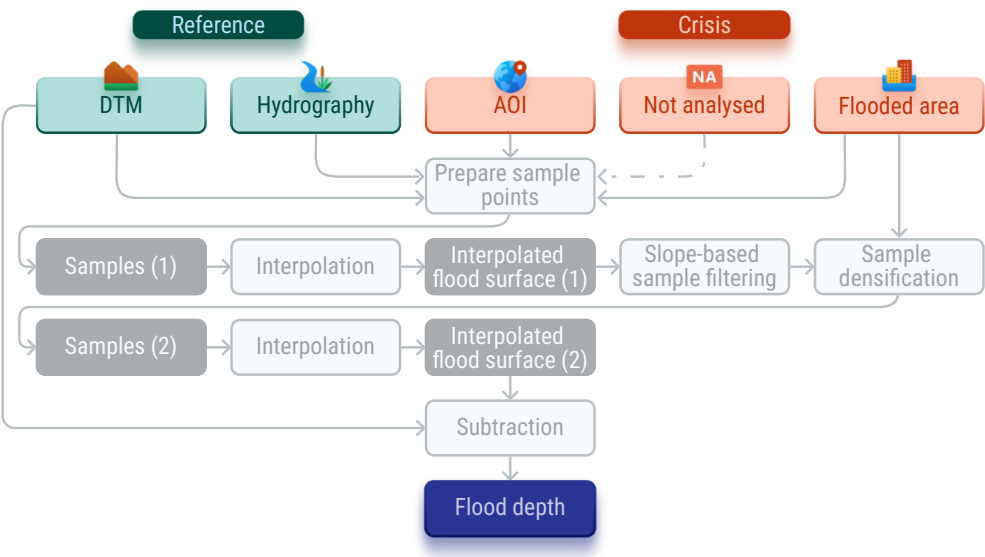


Figure 3. Simplified workflow and data model for INFLOS.

Table 1 presents the required and optional datasets for INFLOS. The combination of flooded area data and hydrographic information indicates the full water extent. Hydrography data is typically sourced from open-source spatial databases, such as OpenStreetMap, or national topographic repositories. Consequently, flooded areas are derived by subtracting hydrography from the overall water extent. In addition to these mandatory datasets, operators can provide ancillary features that define the domain inside which flood depths are estimated. These include the AOI and any areas within the AOI that were not analysed due to incomplete crisis imagery coverage. They are essential for reducing the computation time and removing edge samples.

Table 1. List of required and optional input datasets for INFLOS.

Dataset	Acquisition	Comment
Elevation data	Downloaded from available sources (end-user, CORDA, FABDEM [30], etc.)	Highest available resolution
Hydrography	Downloaded from OpenStreetMap, digitised from reference imagery	Refinement might be necessary
AOI	Provided by the CEMS RM end-user	Should encompass the whole flooded domain
Not analysed areas	Derived from the AOI and crisis image footprint	Optional, to be provided when applicable
Flooded areas	Derived from crisis image	Should be of appropriate quality

To estimate flood depth, INFLOS is based upon four assumptions, three of which are illustrated in Figure 4:

- (A) Flood depth, referred to as fd , can be determined by initially estimating a flood surface, denoted as fs . This is achieved by subtracting elevation data e from the flood surface. Consequently, $fd = e - fs$. Negative values of fd correspond to areas unaffected by the flood and located outside the boundaries of the observed event layer.
- (B) Flood depth at the edges of flooded areas can be approximated as zero, as described by the equation $fd \approx 0 \Leftrightarrow e \approx fs$ for edge vertices.
- (C) A cross-section of a flooded riverbed or floodplain must be a flat water surface.
- (D) It is not possible to consistently infer the bathymetry of hydrological features or the corresponding water depth from the various DTM specifications made available during flood activations.

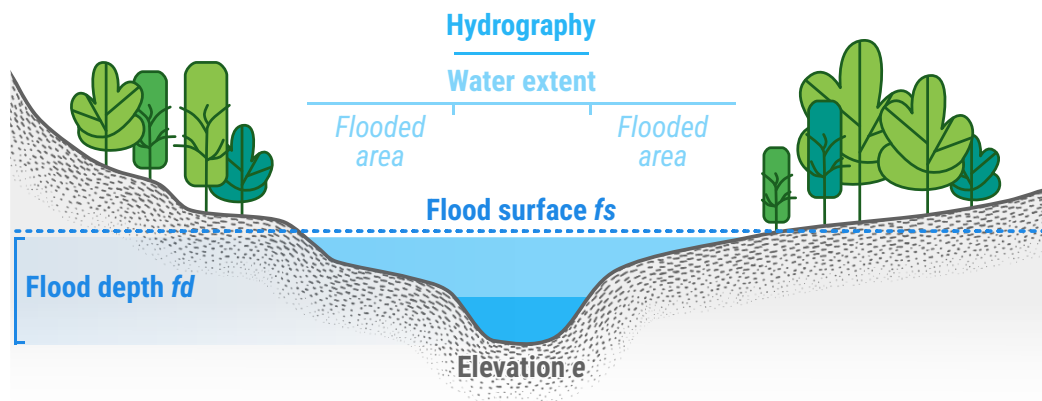


Figure 4. Cross-section of a watercourse, illustrating terminology and concepts used for describing flood depth. It includes hydrography and elevation, available to the operator as inputs. INFLOS generates a flood surface estimate, used to derive flood depth.

The proposed methodology involves a two-stage interpolation process, consisting of the following steps: (1) preparation of sample points and outlier filtering, (2) first-pass interpolation to generate a preliminary flood surface, (3) removal of additional outliers and densification of robust samples, (4) second-pass interpolation where the final flood surface is estimated, and (5) flood depth computation.

2.1. Sample Point Preparation

INFLOS operates on the basis of interpolating a flood surface using a set of sample points located along the edges of flooded areas, where the water depth can be approximated to zero, as per assumptions (A) and (B). The distance between samples is contingent upon the resolution of the crisis image, allowing for an adaptive technique that is applicable across a wide range of sensors. This sampling process is illustrated in Figure 5. Furthermore, it can be extended to include hydrography features adjacent to flooded areas, leading to a more accurate representation of the flood domain. This could potentially enable bathymetry estimation from suitable elevation data.

In line with assumption (B), it is recommended to select only samples located on the periphery of the full water extent for analysis. It can be reasonably assumed that samples situated within this domain will have non-zero positive depth values. Consequently, all samples situated along the boundaries where both the flooded areas and hydrography converge are excluded. Furthermore, samples extracted from flooded areas and positioned near or beyond the limits of the AOI or image footprint are also removed, as they do not align with the actual limits of the observed water extent (Figure 5). This selective sampling methodology ensures an accurate representation of the actual event.

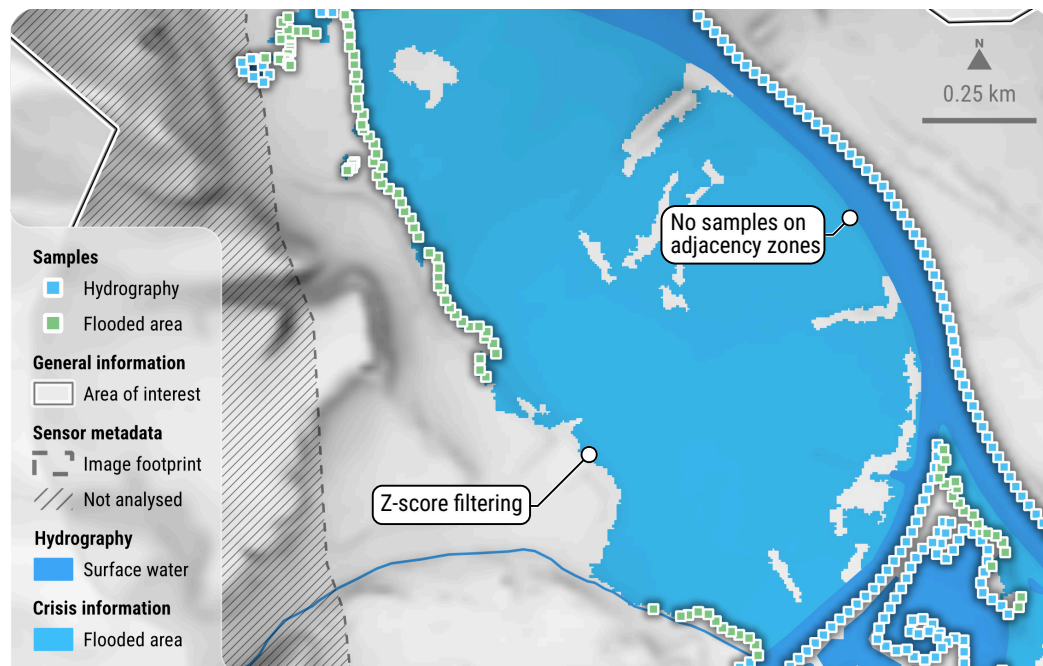


Figure 5. Spatial distribution of sample points, prior to the initial interpolation phase. Each point retrieves its elevation value directly from a DTM. This example is based on an on-demand CEMS RM delineation product delivered for EMSR722 AOI02. All related products can be accessed through the official viewer for EMSR722: <https://rapidmapping.emergency.copernicus.eu/EMSR722/>.

After completing the sampling process, the elevation of each point is calculated using the DTM. In the context of rapid mapping, the reliability of elevation data may not be guaranteed entirely, even with the utmost operator expertise. As a result, the accuracy of mapped water boundaries could be locally inconsistent. This issue is particularly prevalent in Synthetic Aperture Radar (SAR) imagery, where radar shadows from features like hedges can be misleading, as they may resemble water due to similar amplitude values.

To address these challenges, INFLOS has been developed to handle minor inconsistencies in both elevation data and flood delineation. However, significant inaccuracies must be rectified by the operator before proceeding with the rest of the workflow, to guarantee the accuracy and reliability of flood depth values. Pre-processing steps are implemented to remove potential height value outliers among the sampling points. To achieve this, INFLOS uses a per-feature filtering technique based on the standard score, or z-score, of sample elevations. Any z-score deviation greater than 1 from a feature's mean is considered an outlier and is removed, retaining only the most optimal 68 % of the initial set of sample points. Afterwards, statistical techniques are employed to ensure a consistent sample density across flooded areas. This threshold can be adjusted based on the specific hydro-geomorphological characteristics of the floodplain and data quality, allowing for a more accurate representation of complex landscapes.

2.2. First Pass Interpolation

The sample set obtained from the previous step is used to interpolate a flood surface. This interpolation process involves propagating elevation data from the sample points to a broader domain of interpolation, which is typically defined by the convex hull of all sample points. Various interpolation techniques are available, each with specific trade-offs in terms of accuracy, smoothing, parameterisation, and processing speed, among other factors [31,32].

The Nearest Neighbour interpolation method is the simplest and fastest [33], making it suitable for rapid mapping. It assigns the elevation of the nearest sample point to each unsampled location in the interpolation domain. While computationally efficient, this approach frequently results in

a stepped surface appearance, particularly evident in complex geographical areas like entrenched valleys. Furthermore, the reliance on the nearest sample renders it particularly susceptible to outliers. To address these issues, FwDET employs a modified version of this algorithm, where the average elevations of neighbouring samples are iteratively assigned to unsampled areas within a moving window.

Alternative methods were also explored, such as Inverse Distance Weighting (IDW) [34] and Kriging [35]. Both techniques have their advantages and disadvantages for rapid mapping. Indeed, IDW relies on fixed parameters that must be empirically determined by the operator, potentially introducing biases. Kriging provides statistically sound estimates but is computationally intensive, making it impractical for large AOIs under tight time constraints.

Accordingly, INFLOS uses the Natural Neighbour algorithm, which is based on the principles of Voronoi tessellation [36]. This method identifies the nearest subset of samples to an unsampled point and calculates interpolated values by weighting the elevations based on their proportional areas [37]. This results in a more refined interpolation surface, compared to the Nearest Neighbour interpolation, while being more adaptable to local sample variations. Consequently, the Natural Neighbour algorithm is a more robust option for the timely and accurate mapping of flood depths, despite higher computational requirements.

2.3. Sample Refinement and Densification

After the initial interpolation of the flood surface, the sampling set undergoes further refinement to guarantee accuracy and robustness. As stated in assumption (C), the cross-sections of the interpolated flood surface should approximate a flat profile. To achieve this, samples that introduce excessive slope in the flood surface, defined by a threshold of 0.5° , are identified and removed. This step is crucial, because slope within the flood surface may indicate anomalous data points, which could lead to inaccurate flood depths.

Subsequently, this curated dataset is densified to improve the robustness and smoothness of the interpolated flood surface. This is achieved by meshing flooded areas and extracting vertices from this mesh (Figure 6). Vertex density is proportional to the spatial resolution of the crisis image, thus enabling an adaptive process. Additional points are added along the buffered geometry of the water extent to maintain a flat flood surface plane and prevent edge effects. All these points are assigned an elevation value based on the neighbouring sample points using an IDW criterion, before being integrated back into the full sample set. This step not only helps generate a smooth flood surface on the edges, but also minimizes the influence of remaining outliers by increasing the density of data points.

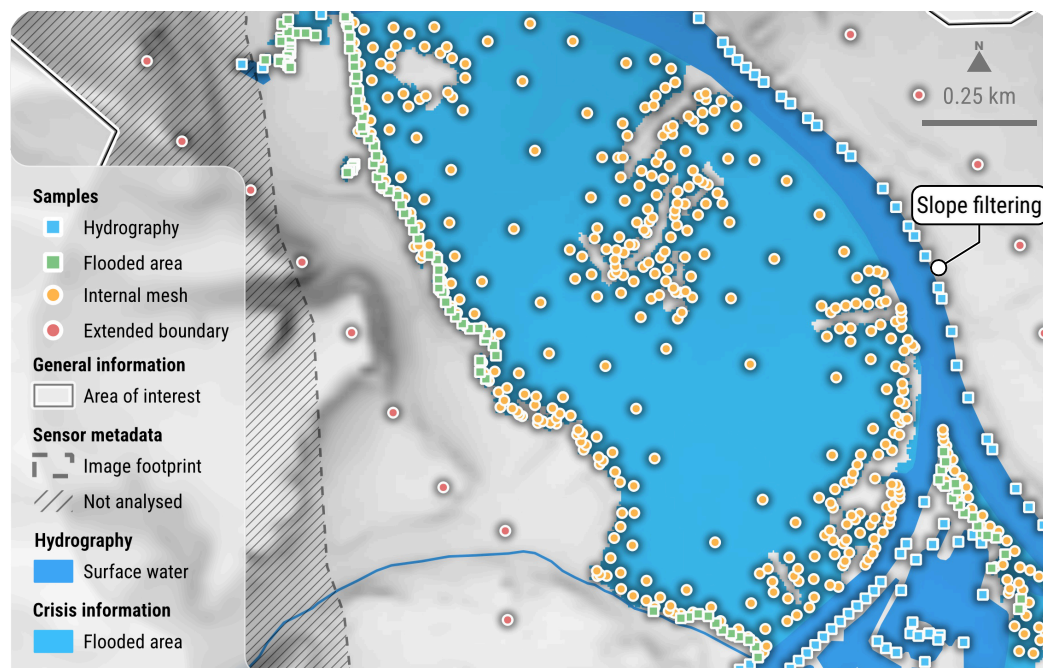


Figure 6. Spatial distribution of sample points, following the application of outlier filtering and densification techniques, represents the data set before the second pass interpolation. Elevations derived from internal meshing and boundary extension are obtained directly from their nearest hydrography and flooded area neighbour samples. This example is based on an on-demand CEMS RM delineation product delivered for EMSR722 AIOI02. All related products can be accessed through the official viewer for EMSR722: <https://rapidmapping.emergency.copernicus.eu/EMSR722/>.

2.4. Second-Pass Interpolation and Flood Depth Computation

The final flood surface is obtained by applying the Natural Neighbour interpolation a second time, using the curated sample set as an input. The elevation values from the DTM are then subtracted from the flood surface, resulting in the depth values associated with the flooding. These depth values are only calculated for flooded areas, excluding the hydrographic data, as previously stated in assumption (D). Minor discrepancies between the crisis image and the elevation data could result in negative or zero depth values. To address this, a minimum threshold of 0.15 metres is applied, ensuring that areas identified as flooded have a depth of at least 0.15 metres.

Next, a series of formatting procedures are undertaken to produce a layer that adheres to the standards and guidelines of CEMS RM. The flood depth values are distributed as a continuous raster file. To obtain vector layers, the data is then discretised into the following classes: below 0.50 m, 0.50 m to 1.00 m, 1.00 to 2.00 m, 2.00 m to 4.00 m, 4.00 m to 6.00 m, and above 6.00 m. This discrete representation is then converted and shared in vector format.

2.5. Validation and Quality Assessment

A significant challenge in the validation process for INFLOS is the absence of robust in-situ data, which is crucial for validating flood depth values. This gap arises from the scarcity of validated, precise in-situ measurements that can accurately represent flood extents and depths at specific moments, corresponding to the acquisition date and time of crisis satellite imagery.

Regarding the validation of results through the use of traditional flood modelling techniques, although hydraulic simulations offer a potential avenue for assessing INFLOS interpolation results, this approach requires considerable effort and reduces the number of flood products that can be verified. This may compromise the validity of the results, considering the variety and number of CEMS RM activations. Furthermore, hydraulic models have inherent limitations and depend on input data

quality, which may not consistently capture the nuances of observed flood events or align with the CEMS RM data model.

Alternative data sources, such as traditional and social media, alongside water gauge readings, offer supplementary validation avenues. However, these sources often lack precise timestamps and geolocations, reducing their reliability in matching the exact conditions and timing of satellite image acquisitions during a crisis. Nevertheless, they can indicate whether an area was flooded and to what extent.

Given these limitations, it is unrealistic to expect highly precise flood depths from INFLOS, as the system is primarily designed for rapid mapping to provide a situational overview for emergency management. Therefore, the primary metric for quality assessment during the validation process is the flatness of the interpolated flood surface, as well as the coherence of the inferred values when compared to elevation data. This criterion aligns with assumption (C), suggesting that a flatter surface indicates higher confidence in the result. Consequently, the quality assessment of INFLOS involves analysing cross-sections where both the DTM and the interpolated flood surface are compared. Figure 4 demonstrates this approach, illustrating how the flood surface f_s and elevation e would be overlaid in a Geographical Information System (GIS) suite for analysis.

3. Implementing the Algorithm and Results

3.1. Development Stage Overview

The development of INFLOS has been structured through multiple stages, categorised by the Technological Readiness Level (TRL) framework [38]. In a period of six months, INFLOS progressed from a proof of concept at TRL 3 to a mature solution for flood depth estimation at TRL 9. This progression involved rigorous testing across diverse landscapes, using a large range of flooded case studies derived from satellite images and elevation datasets.






Initial tests focused on single-date flood depth estimations within a constrained set of use cases. As development progressed, the scope expanded to include monitoring phases that accounted for fluctuating water extents and levels across the same AOIs at first. This process gradually incorporated a broader spectrum of use cases into the evaluation process.

These development stages led to the operational deployment of INFLOS into the CEMS RM toolkit. All partners within the CEMS RM consortium successfully used INFLOS to generate numerous flood depth products in real-world operational settings. This phased approach not only validated the performance of INFLOS across different scenarios, but also ensured its adaptability and robustness, reinforcing its value as a critical tool in flood response and management strategies.

3.2. Proof of Concept

Initially, INFLOS was tested on single-date flood products to validate the accuracy of the interpolated flood surfaces, ensuring they maintained near-flat profiles across various configurations. This testing was essential to confirm that the computed flood depths aligned with the elevations indicated by DTMs, regardless of the geographical features present within the event area. Consequently, the testing encompassed a diverse range of geographical settings, from narrow, deep valleys to large open plains, as detailed in Table 2. This comprehensive approach aimed to reflect the diversity of flood activations and related events within the CEMS RM framework.

Table 2. List of CEMS RM activations used for conceptualising, developing and testing INFLOS in an experimental setting. All related products are accessible through the CEMS RM portal: <https://emergency.copernicus.eu/mapping/list-of-activations-rapid>.

Activation	Locality	AOI	Event size (ha)	Description
EMSR692	 Greece	01	72 200	Succession of flat and entrenched areas, major elevation amplitude, artefacts in DTM, multi-stage flooding, long monitoring
EMSR698	 United Kingdom	01	2190	Long and entrenched valley, major elevation amplitude, multi-stage flooding
EMSR705	 Italy	03	1635	Flat landscape, artefacts in DTM
EMSR706	 France	04	700	Flat landscape
EMSR708	 Belgium	01	5300	Flat landscape, coastal area

Once INFLOS demonstrated sufficient stability for broader applications, the testing phase expanded to include monitoring cycles for all products in Table 2. This phase was critical to validate that INFLOS could accurately account for dynamic flood events. Specifically, the algorithm was required to demonstrate that the interpolated flood depths logically increased with the expansion of flood extents and decreased as the flooding receded.

To illustrate these capabilities, Figure 7 displays upstream and downstream cross-sections that were generated for the Spey River in Scotland, as part of the EMSR698 activation. Upriver, the reduction in the flooded area results in a lower flood surface in the DEL MONIT01 generated on 2023-10-10, compared to the initial DEL PRODUCT from 2023-10-08. As per assumption (C), these interpolated flood surfaces are expected to be nearly flat, exhibiting slopes close or equal to 0°. Despite vertical exaggerations in the profile visualizations in Figure 7, the slopes for flood surfaces in DEL PRODUCT and DEL MONIT01 are measured at 0.018° and 0.047°, respectively. This minimal variation across each profile supports the assumption of flat flood surfaces. Downriver, as the inundation extends, flooded areas in DEL MONIT01 display a broader extent, resulting in increased flood depth estimates, compared to the earlier DEL PRODUCT. The profiles remain nearly uniform and consistent with the flatness criterion, showing flood surface slopes of −0.056° for DEL PRODUCT and −0.017° for DEL MONIT01.

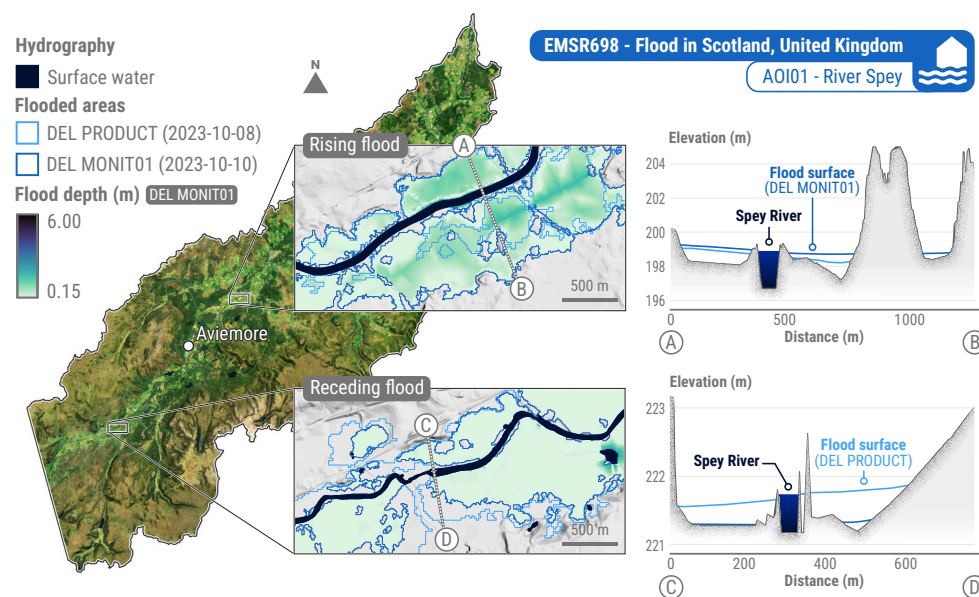


Figure 7. Cross-sections with rising and receding floodwater, along the Spey River in Scotland. The DEL PRODUCT (2023-10-08) and DEL MONIT01 (2023-10-10) flooded areas illustrate how the inundation has progressed downstream. The flood surface is a sum of elevation data and interpolated flood depth. Most artefacts in the flood depth layer are due to the DTM quality. This example draws from on-demand CEMS RM products delivered for EMSR698 AOI01. All related products can be accessed through the official viewer for EMSR698: <https://rapidmapping.emergency.copernicus.eu/EMSR698/>.















The validation process was applied across all use cases listed in Table 2, yielding consistent results regardless of the geographical or hydrological context. This preliminary assessment, conducted under conditions similar to those in the CEMS RM framework, facilitated INFLOS' progress towards a TRL of 5. At this stage, the proposed methodology demonstrated its effectiveness in a relevant environment, providing a solid basis for further enhancements and optimisations necessary for full operational deployment.

3.3. Pre-Operational Environment

The transition of INFLOS to a pre-operational stage involved an update in employed technologies. Initially, the proof of concept was conducted using ArcGIS Pro model builders, enabling rapid iteration across various use cases. After validating the methodology, the workflow was transferred to Jupyter Notebooks [39] and subsequently refined into standalone Python scripts, accommodating both ESRI and open-source platforms, notably incorporating WhiteboxTools [40] for its implementation of the Natural Neighbour algorithm, as well as geopandas [41], xarray [42] and sertit-utils [43]. This adaptability facilitated the integration of INFLOS into diverse technical environments, making it accessible via command line for advanced users and through a graphical user interface in ArcGIS Pro for a more general use.

Following this adaptation, INFLOS was shared among CEMS RM partners, initiating an extensive testing phase that involved processing 14 activations, with over 180 flood products (Table 3). This was crucial not only for operational benchmarking, but also for ensuring compatibility across the varied IT infrastructures within the CEMS RM consortium. Feedback from partners played a vital role in this phase, identifying areas for improvement and issues, which were addressed in subsequent updates.

Table 3. List of non-sensitive CEMS RM activations used in the pre-operational environment, with the corresponding number of generated delineation products, including monitoring. All related products are accessible through the CEMS RM portal: <https://emergency.copernicus.eu/mapping/list-of-activations-rapid>.

Activation	Locality	Number of AOIs	Number of products
EMSR692	 Greece	7	28
EMSR697	 Greece	4	2
EMSR698	 United Kingdom	3	5
EMSR705	 Italy	8	7
EMSR706	 France	7	15
EMSR708	 Belgium	3	8
EMSR711	 France	3	4
EMSR712	 Germany	10	71
EMSR713	 Germany	1	1
EMSR718	 Ireland	2	2
EMSR720	 Brazil	5	7
EMSR722	 Germany	2	7
EMSR725	 Sweden	4	3
EMSR728	 Germany	10	23

This approach not only strengthened the tool’s robustness but also enabled an assessment of INFLOS’ performance in terms of execution time, a critical metric for its suitability in rapid mapping scenarios. Initial benchmarking was conducted internally at SERTIT, using a standard desktop computer setup equipped with an 8-core 3.60 GHz CPU and 32 GB of RAM. This configuration aimed to simulate a typical user environment, providing realistic performance insights. The median processing time using INFLOS was recorded at 5.2 minutes, highlighting its efficiency in managing datasets under typical CEMS RM operational conditions. Processing times varied significantly depending on the AOI, data complexity, and output size. The longest was 30.4 minutes for EMSR723 AOI01, which involved a large area of 527 668 ha, resulting in a raster size of 30 469 × 17 676 pixels. This scenario tested the tool’s capacity to handle extensive data volumes under demanding conditions. The quickest processing time was notably brief at approximately 0.4 minutes for EMSR720 AOI03, with a small raster size of 217 × 146 pixels, for an area of 4633 ha.

The collaborative testing and refinement of INFLOS underscored its potential to meet end-user requirements in emergency mapping operations, with a TRL of 7, paving the way for full-scale production deployment.

3.4. Operational Production

The integration of INFLOS into the CEMS RM portfolio required adhering to data models, symbology, and processing protocol requirements. This ensures that the outputs from INFLOS are not only thematically accurate, but also seamlessly fit into the existing operational framework. Flood depth is distributed in the Crisis Information Package (CIP) as a continuous raster layer and a classified vector file. This dual-format delivery ensures versatility in usage, catering to different user needs and technical environments. The raster format enables detailed quantitative analyses, while the vector format facilitates integration and visualization within various GIS platforms. Moreover, a standardized symbology has been developed, enhancing the readability and usability of flood maps. This includes defining colour scales that accurately represent water depth, making it intuitive for end-users to interpret the severity and extent of flooding directly from the map. Figure 8 demonstrates the finalised integration of INFLOS into the CEMS RM portfolio, showcasing a flood delineation monitoring product for EMSR720 in Brazil.

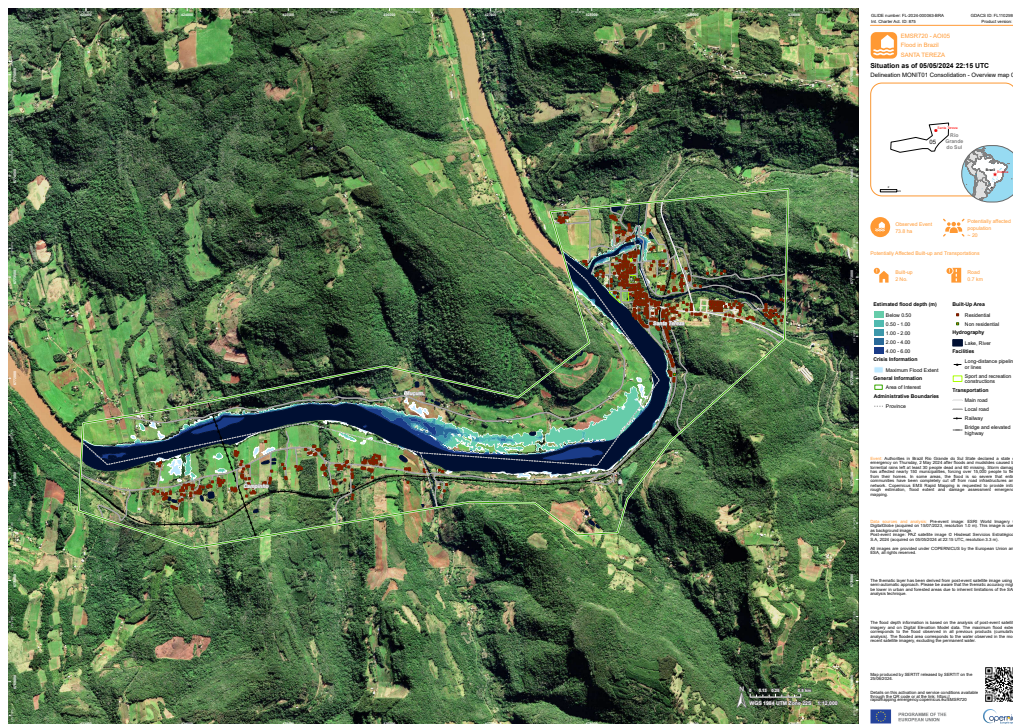


Figure 8. Example of an on-demand CEMS RM delineation monitoring product. This ready-to-print map was generated for EMSR720 AOI05, following inundations in May 2024, in the Brazilian State of Rio Grande do Sul. It shows the current and maximum extent of the flood, as well as an estimate of flood depth. All related products can be accessed through the official viewer for EMSR720: <https://rapidmapping.emergency.copernicus.eu/EMSR720/>.

As a result of the comprehensive development phase, INFLOS has evolved into a fully operational system (TRL 9), being utilized for all delineation products within CEMS RM, and effectively tracking fluctuations in flood events over time.

4. Discussion

INFLOS demonstrates an efficient capability to derive flood depths from flood extents delineated using remote sensing imagery and elevation data within the context of CEMS RM. Tested across over 180 products, INFLOS has shown remarkable adaptability to a wide range of input data and diverse terrain configurations, highlighting its suitability in an operational setting. The tool effectively processes imagery with varying resolutions, sourced from both optical and SAR sensors. Even though INFLOS is compatible with medium-resolution DTMs such as FABDEM at 30 m, there is a preference for finer grid cell sizes. Indeed, HR or VHR DTMs can significantly enhance the accuracy of flood depth estimates by capturing the intricate topographical variations often found in flood-prone areas [44]. Nevertheless, the outcomes are also influenced by the DTM's quality, as well as processing techniques such as tile mosaicking, which can lead to poor interpolations.

While INFLOS meets the original operational requirement of processing within a 30-minute timeframe, the increasing scale and frequency of major disasters [45] suggests a potential rise in the size of AOIs and flooded areas needing analysis. FwDET is a comparable tool that demonstrates potentially faster computation times than INFLOS. However, this comes at the cost of omitting its smoothing post-process, which enhances the quality of the flood surface representation. Indeed, FwDET's post-processing involves an iterative low-pass filter to smooth the derived flood surfaces. The typical range for these iterations is between 100 and 200, which significantly influences the final output quality and computation time [27]. To assess the performance trade-offs between INFLOS and FwDET, 21 products were selected from Table 3 for benchmarking. These tests were conducted under two scenarios for FwDET, without any post-processing iterations—0 iterations—and with 150

iterations. Figure 9 shows the results of this benchmark, using a desktop computer with an 8-core 3.60 GHz CPU and 32 GB of RAM.

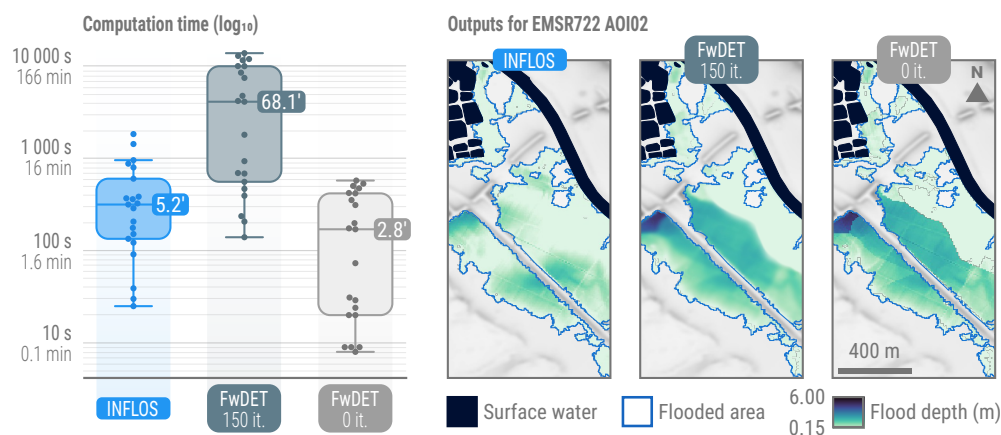


Figure 9. Benchmarking of INFLOS, compared to FwDET with 0 and 150 iterations. For enhanced visual clarity, computation times are presented on a logarithmic scale. Snapshots from EMSR722 AOI01 - DEL PRODUCT illustrate typical flood depth outcomes when using these techniques. All related products can be accessed through the official viewer for EMSR722: <https://rapidmapping.emergency.copernicus.eu/EMSR722/>.

Without any post-processing, FwDET operates faster than the proposed methodology, achieving a median computation time of 2.8 minutes compared to INFLOS' 5.2 minutes. This difference in processing speed is further highlighted by INFLOS' computation times that vary significantly, ranging from 0.4 to 30.4 minutes and scaling poorly with AOI size as well as terrain complexity. In contrast, FwDET (0 it.) maintains a narrower range of 0.1 to 9.5 minutes, showcasing its better scalability. However, introducing a low-pass filter to FwDET to improve surface smoothness negatively influences its efficiency. With 150 iterations, FwDET's median computation time increases up to 68.1 minutes, which is considerably longer than the maximum processing time observed for INFLOS even on the largest AOI and event size.

As illustrated in Figure 9, INFLOS generates smooth inundation surfaces without discontinuities, resulting in more accurate flood depth simulations. This enhanced precision is achieved through the use of the Natural Neighbour interpolation algorithm, which considers the surrounding samples for each interpolated point, effectively integrating a built-in smoothing pass [37]. In comparison, FwDET relies on the Nearest Neighbour algorithm [27], producing tessellated and disjointed surfaces that do not convincingly simulate water behaviour. This approach results in less accurate flood mapping, especially evident in complex terrains. This is reflected in Figure 9 by significant and discrete changes in flood depths. Although the low-pass filter mitigates this issue to some extent, its impact on computation time reduces FwDET's usability in rapid mapping contexts. However, while INFLOS currently has a clear advantage in terms of relevance, the time gap with FwDET (0 it.) suggests areas for improvement. One potential avenue could be exploring alternative interpolation techniques that maintain the quality of flood surface representation while reducing computational overhead. Currently, both interpolation passes account for over 80 % of INFLOS' runtime, making such a change crucial for its operational suitability.

Nonetheless, any modifications to the interpolation technique used by INFLOS should adequately address outliers. Even with the existing outlier removal procedures, the proposed methodology is particularly sensitive to input data precision, particularly over- and under-estimations of flooded areas. Careful cleaning of the flood delineation is essential to maintain the accuracy of the outputs. In any event, satellite and aerial-based water extractions remain challenging in natural landscapes, especially in riparian and forested areas (Figure 10). Water hidden beneath dense vegetation can be

significantly under-detected. Standard outlier filtering techniques struggle to capture these submerged areas, as they often remain invisible in optical imagery and are challenging to delineate even in SAR imagery due to canopy backscatter. Another critical issue arises from SAR imagery, where shadows cast by topography and trees share similar amplitudes to water surfaces, which have low values due to specular reflection. These discrepancies can lead to aberrant flood depths, especially when false positives are located upslope outside flood-prone areas, by locally pulling the interpolation plane upwards.

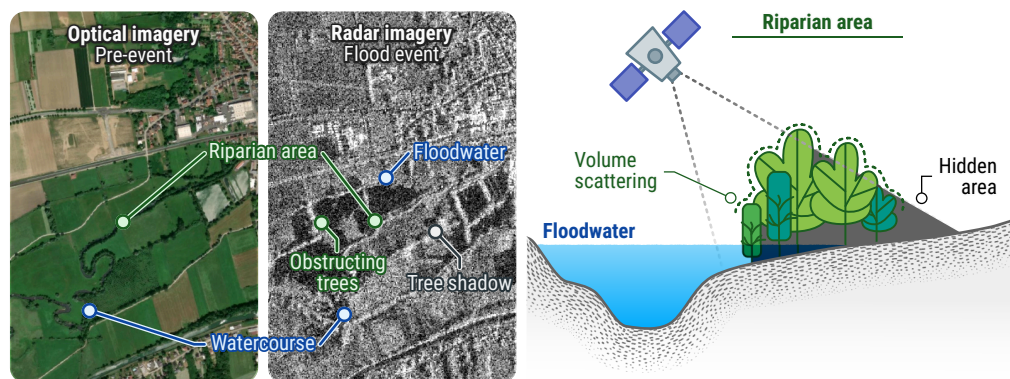


Figure 10. Limits to flood mapping using remote sensing in semi-natural and forested areas. Floods can be hidden by canopy, with the sensors available as part of crisis activities. In addition, tall vegetation can block incident signal, causing shadows whose backscatter or lack thereof is similar to that of water.

Urban environments present challenges for flood mapping as well, due to their complex geometry and dense structures. Optimal flood mapping in these areas requires the use of VHR imagery, captured at a nadir angle, to improve visibility in street corridors. However, SAR sensors are inherently side-looking and often face difficulties in this setting. Street geometry can lead to multiple backscatter rebounds off of angular surfaces like buildings, causing strong return signals that may mask the presence of floodwater (Figure 11). Additionally, less dense settlements experience radar shadowing from buildings and other tall features.

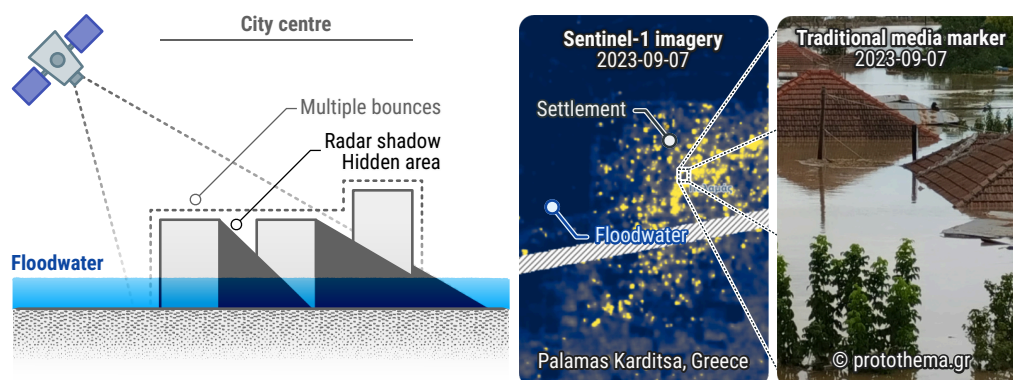


Figure 11. Limits to flood mapping using remote sensing in an urban context. This example pertains to EMSR692, an activation triggered following inundations in Greece. The Sentinel-1 imagery shows a high backscatter in the municipality of Palamas Karditsa, even though it was entirely flooded as per various sources. Media data was collected and made available by Hensoldt AG. All related products can be accessed through the official viewer for EMSR692: <https://rapidmapping.emergency.copernicus.eu/EMSR692/>.

Recent techniques proposed by Chini et al. (2019) [46] leverage Sentinel-1 interferometry to mitigate these issues, demonstrating the potential of interferometry in urban flood mapping. Radar interferometry can discern subtle elevation changes by analysing the phase differences between SAR

images acquired at different times [47], potentially indicating the presence of water in settlements. However, incorporating interferometry into rapid mapping workflows would require additional effort to assess repeatability, performance and timeliness. To address some of the limitations of remote sensing and INFLOS, SERTIT has initiated the development of an extrapolation tool called EXFLOS (EXtrapolated FLOOD Surfaces) within the framework of CEMS RM. The purpose of EXFLOS is to support the parametric flooding of various landscapes, including urban settlements or vegetated areas, while still leveraging the original layers mentioned in Table 1. The EXFLOS tool is still in the development and validation phase, and will be presented in a separate publication.

5. Conclusion

INFLOS is a new methodology that has been proposed for estimating flood depth within the context of CEMS RM. Conceptualised independently of similar solutions, INFLOS has undergone a series of development stages, evolving from a proof of concept to a mature and operational solution. This progression involved rigorous testing across various landscapes, crisis imagery from optical and SAR sensors, and diverse DTM datasets. This phased approach not only validated the performance of INFLOS across different scenarios, but also ensured its adaptability and robustness, reinforcing its value as a critical tool in flood response and management strategies. The initial proof of concept focused on single-date flood product testing, ensuring the consistency of the interpolated flood surfaces with DTM elevations. This was followed by the expansion of testing to include monitoring cycles, which validated INFLOS' ability to account for dynamic flood events accurately. The subsequent shift towards a pre-operational stage involved adapting the system to diverse technical environments, making it accessible through both command line and graphical user interfaces. Extensive testing and refining in this phase not only enhanced the tool's robustness but also allowed for an evaluation of its performance with respect to comparable solutions such as FwDET. Execution time, a critical metric for its applicability in rapid mapping scenarios, was also extensively tested and optimised. The system's final integration into CEMS RM demonstrates its maturity, making it an operational tool used for all delineation products, including monitoring phases. In summary, INFLOS has undergone a comprehensive development process, resulting in a robust and effective tool for flood depth estimation. Its validated performance and adaptability make it a valuable asset in flood response and management strategies, contributing to more efficient and accurate emergency mapping operations.

Author Contributions: Conceptualisation, A.C.; methodology, A.C., R.B., Q.P. and S.C.; software, R.B. and Q.P.; validation, P.C., C.H., A.C., Q.P. and R.B.; writing—original draft preparation, Q.P., S.C. and A.C.; writing—review and editing, Q.P., S.C., P.C. and A.C.; visualisation, Q.P.; supervision, S.C. and P.C. All authors have read and agreed to the published version of the manuscript.

Acknowledgments: We would like to express our gratitude to the Joint Research Centre for their support and guidance in the development of this methodology, more specifically Pietro Ceccato, Jean-François Pekel, Alan Steel, Paolo Pasquali, Simone Dalmasso, Inès Joubert-Boitat and Oliva Martin Sanchez. Their expertise and insights have been invaluable, and this work would not have been possible without their contribution. We are also grateful to our CEMS RM partners with a special mention to e-GEOS, the project's prime contractor, as well as team members CLS, GAF AG, GMV, IABG, Ithaca, Planetek Hellas, TPZ Iberica and SERTIT, for their active engagement and operational use of INFLOS. Their practical application of the tool has provided us with invaluable insights, which have led to significantly enhancing the robustness and relevance of our work.

References

1. Tarasova, L.; Lun, D.; Merz, R.; Blöschl, G.; Basso, S.; Bertola, M.; Miniussi, A.; Rakovec, O.; Samaniego, L.; Thober, S.; Kumar, R. Shifts in flood generation processes exacerbate regional flood anomalies in Europe. *Communications Earth & Environment* **2023**, *4*, 49. doi:10.1038/s43247-023-00714-8.
2. Delforge, D.; Wathelet, V.; Below, R.; Sofia, C.L.; Tonnelier, M.; Loenhout, J.v.; Speybroeck, N. EM-DAT: the Emergency Events Database. Technical report, Research Square Platform LLC, 2024. doi:10.21203/rs.3.rs-3807553/v1.
3. Blöschl, G.; Hall, J.; Viglione, A.; Perdigão, R.A.P.; Parajka, J.; Merz, B.; Lun, D.; Arheimer, B.; Aronica, G.T.; Bilibashi, A.; Boháč, M.; Bonacci, O.; Borga, M.; Čanjevac, I.; Castellarin, A.; Chirico, G.B.; Claps, P.; Frolova,

- N.; Ganora, D.; Gorbachova, L.; Gül, A.; Hannaford, J.; Harrigan, S.; Kireeva, M.; Kiss, A.; Kjeldsen, T.R.; Kohnová, S.; Koskela, J.J.; Ledvinka, O.; Macdonald, N.; Mavrova-Guirguinova, M.; Mediero, L.; Merz, R.; Molnar, P.; Montanari, A.; Murphy, C.; Osuch, M.; Ovcharuk, V.; Radevski, I.; Salinas, J.L.; Sauquet, E.; Šraj, M.; Szolgay, J.; Volpi, E.; Wilson, D.; Zaimi, K.; Živković, N. Changing climate both increases and decreases European river floods. *Nature* **2019**, *573*, 108–111. doi:10.1038/s41586-019-1495-6.
4. Rentschler, J.; Salhab, M. People in Harm's Way: Flood Exposure and Poverty in 189 Countries. Technical report, World Bank, Washington, DC, 2020. doi:10.1596/1813-9450-9447.
 5. Makhnovsky, D. The Coastal Regions of Europe: Economic Development at the Turn of the 20th Century. *Baltic Region* **2014**, *4*, 50–66. doi:10.5922/2079-8555-2014-4-4.
 6. European Commission. Eurostat. *Eurostat regional yearbook 2011*; Publications Office: LU, 2011.
 7. Kumm, M.; De Moel, H.; Ward, P.J.; Varis, O. How Close Do We Live to Water? A Global Analysis of Population Distance to Freshwater Bodies. *PLoS ONE* **2011**, *6*, e20578. doi:10.1371/journal.pone.0020578.
 8. United Nations. *World urbanization prospects: the 2018 revision*; United Nations: New York, 2019. OCLC: 1120698127.
 9. Notti, D.; Giordan, D.; Caló, F.; Pepe, A.; Zucca, F.; Galve, J.P. Potential and Limitations of Open Satellite Data for Flood Mapping. *Remote Sensing* **2018**, *10*, 1673. doi:10.3390/rs10111673.
 10. Boccardo, P.; Giulio Tonolo, F. Remote Sensing Role in Emergency Mapping for Disaster Response. In *Engineering Geology for Society and Territory - Volume 5*; Lollino, G.; Manconi, A.; Guzzetti, F.; Culshaw, M.; Bobrowsky, P.; Luino, F., Eds.; Springer International Publishing: Cham, 2015; pp. 17–24. doi:10.1007/978-3-319-09048-1_3.
 11. Munawar, H.S.; Hammad, A.W.A.; Waller, S.T. Remote Sensing Methods for Flood Prediction: A Review. *Sensors* **2022**, *22*, 960. doi:10.3390/s22030960.
 12. Ajmar, A.; Boccardo, P.; Broglia, M.; Kucera, J.; Giulio-Tonolo, F.; Wania, A. Response to Flood Events: The Role of Satellite-based Emergency Mapping and the Experience of the Copernicus Emergency Management Service. In *Geophysical Monograph Series*, 1 ed.; Molinari, D.; Menoni, S.; Ballio, F., Eds.; Wiley, 2017; pp. 211–228. doi:10.1002/9781119217930.ch14.
 13. Brunner, G.W. HEC-RAS river analysis system. Hydraulic reference manual. Version 1.0. Technical report, Hydrologic Engineering Center, 1997.
 14. Van Der Knijff, J.M.; Younis, J.; De Roo, A.P.J. LISFLOOD: a GIS-based distributed model for river basin scale water balance and flood simulation. *International Journal of Geographical Information Science* **2010**, *24*, 189–212. doi:10.1080/13658810802549154.
 15. Erena, S.H.; Worku, H.; De Paola, F. Flood hazard mapping using FLO-2D and local management strategies of Dire Dawa city, Ethiopia. *Journal of Hydrology: Regional Studies* **2018**, *19*, 224–239.
 16. Dimitriadis, P.; Tegos, A.; Oikonomou, A.; Pagana, V.; Koukouvinos, A.; Mamassis, N.; Koutsoyiannis, D.; Efstratiadis, A. Comparative evaluation of 1D and quasi-2D hydraulic models based on benchmark and real-world applications for uncertainty assessment in flood mapping. *Journal of Hydrology* **2016**, *534*, 478–492. doi:10.1016/j.jhydrol.2016.01.020.
 17. Hunter, N.M.; Bates, P.D.; Neelz, S.; Pender, G.; Villanueva, I.; Wright, N.G.; Liang, D.; Falconer, R.A.; Lin, B.; Waller, S.; Crossley, A.J.; Mason, D.C. Benchmarking 2D hydraulic models for urban flooding. *Proceedings of the Institution of Civil Engineers - Water Management* **2008**, *161*, 13–30. doi:10.1680/wama.2008.161.1.13.
 18. Jamali, B.; Bach, P.M.; Cunningham, L.; Deletic, A. A Cellular Automata Fast Flood Evaluation (CA-ffé) Model. *Water Resources Research* **2019**, *55*, 4936–4953. doi:10.1029/2018WR023679.
 19. Kleyko, D.; Frady, E.P.; Sommer, F.T. Cellular Automata Can Reduce Memory Requirements of Collective-State Computing. *IEEE Transactions on Neural Networks and Learning Systems* **2022**, *33*, 2701–2713. arXiv:2010.03585 [cs], doi:10.1109/TNNLS.2021.3119543.
 20. Gibson, M.J.; Savic, D.A.; Djordjevic, S.; Chen, A.S.; Fraser, S.; Watson, T. Accuracy and Computational Efficiency of 2D Urban Surface Flood Modelling Based on Cellular Automata. *Procedia Engineering* **2016**, *154*, 801–810. doi:10.1016/j.proeng.2016.07.409.
 21. Liu, L.; Liu, Y.; Wang, X.; Yu, D.; Liu, K.; Huang, H.; Hu, G. Developing an effective 2-D urban flood inundation model for city emergency management based on cellular automata. *Natural Hazards and Earth System Sciences* **2015**, *15*, 381–391. doi:10.5194/nhess-15-381-2015.
 22. Hosseiny, H.; Nazari, F.; Smith, V.; Nataraj, C. A Framework for Modeling Flood Depth Using a Hybrid of Hydraulics and Machine Learning. *Scientific Reports* **2020**, *10*, 8222. doi:10.1038/s41598-020-65232-5.

23. Elkhachy, I. Flash Flood Water Depth Estimation Using SAR Images, Digital Elevation Models, and Machine Learning Algorithms. *Remote Sensing* **2022**, *14*, 440. doi:10.3390/rs14030440.
24. Karpatne, A.; Ebert-Uphoff, I.; Ravela, S.; Babaie, H.A.; Kumar, V. Machine Learning for the Geosciences: Challenges and Opportunities, 2017. arXiv:1711.04708 [physics].
25. Cian, F.; Marconcini, M.; Ceccato, P.; Giupponi, C. Flood depth estimation by means of high-resolution SAR images and lidar data. *Natural Hazards and Earth System Sciences* **2018**, *18*, 3063–3084. doi:10.5194/nhess-18-3063-2018.
26. Betterle, A.; Salamon, P. Water depth estimate and flood extent enhancement for satellite-based inundation maps. *Natural Hazards and Earth System Sciences Discussions* **2024**. doi:10.5194/nhess-2024-22.
27. Cohen, S.; Brakenridge, G.R.; Kettner, A.; Bates, B.; Nelson, J.; McDonald, R.; Huang, Y.; Munasinghe, D.; Zhang, J. Estimating Floodwater Depths from Flood Inundation Maps and Topography. *JAWRA Journal of the American Water Resources Association* **2018**, *54*, 847–858. doi:10.1111/1752-1688.12609.
28. Cohen, S.; Raney, A.; Munasinghe, D.; Loftis, J.D.; Molthan, A.; Bell, J.; Rogers, L.; Galantowicz, J.; Brakenridge, G.R.; Kettner, A.J.; Huang, Y.F.; Tsang, Y.P. The Floodwater Depth Estimation Tool (FwDET v2.0) for improved remote sensing analysis of coastal flooding. *Natural Hazards and Earth System Sciences* **2019**, *19*, 2053–2065. doi:10.5194/nhess-19-2053-2019.
29. Maxant, J.; Braun, R.; Caspard, M.; Clandillon, S. ExtractEO, a Pipeline for Disaster Extent Mapping in the Context of Emergency Management. *Remote Sensing* **2022**, *14*, 5253. doi:10.3390/rs14205253.
30. Hawker, L.; Uhe, P.; Paulo, L.; Sosa, J.; Savage, J.; Sampson, C.; Neal, J. A 30 m global map of elevation with forests and buildings removed. *Environmental Research Letters* **2022**, *17*, 024016. doi:10.1088/1748-9326/ac4d4f.
31. Shyamala, G.; Arun Kumar, B.; Manvitha, S.; Vinay Raj, T. Assessment of Spatial Interpolation Techniques on Groundwater Contamination. In *International Conference on Emerging Trends in Engineering (ICETE)*; Satapathy, S.C.; Raju, K.S.; Molugaram, K.; Krishnaiah, A.; Tsihrintzis, G.A., Eds.; Springer International Publishing: Cham, 2020; Vol. 2, pp. 262–269. Series Title: Learning and Analytics in Intelligent Systems, doi:10.1007/978-3-030-24314-2_33.
32. Xu, W.; Zou, Y.; Zhang, G.; Linderman, M. A comparison among spatial interpolation techniques for daily rainfall data in Sichuan Province, China. *International Journal of Climatology* **2015**, *35*, 2898–2907. doi:10.1002/joc.4180.
33. Xing, Y.; Song, Q.; Cheng, G. Benefit of Interpolation in Nearest Neighbor Algorithms. *SIAM Journal on Mathematics of Data Science* **2022**, *4*, 935–956. doi:10.1137/21M1437457.
34. Lu, G.Y.; Wong, D.W. An adaptive inverse-distance weighting spatial interpolation technique. *Computers & Geosciences* **2008**, *34*, 1044–1055. doi:10.1016/j.cageo.2007.07.010.
35. Oliver, M.A.; Webster, R. Kriging: a method of interpolation for geographical information systems. *International journal of geographical information systems* **1990**, *4*, 313–332. doi:10.1080/02693799008941549.
36. Sibson, R. A vector identity for the Dirichlet tessellation. *Mathematical Proceedings of the Cambridge Philosophical Society* **1980**, *87*, 151–155. doi:10.1017/S0305004100056589.
37. Ledoux, H.; Gold, C. An Efficient Natural Neighbour Interpolation Algorithm for Geoscientific Modelling. In *Developments in Spatial Data Handling*; Springer-Verlag: Berlin/Heidelberg, 2005; pp. 97–108. doi:10.1007/3-540-26772-7_8.
38. Mankins, J.C.; others. Technology readiness levels. *White Paper, April* **1995**, *6*, 1995.
39. Kluyver, T.; Ragan-Kelley, B.; Pérez, F.; Granger, B.; Bussonnier, M.; Frederic, J.; Kelley, K.; Hamrick, J.; Grout, J.; Corlay, S.; Ivanov, P.; Avila, D.; Abdalla, S.; Willing, C. Jupyter Notebooks – a publishing format for reproducible computational workflows. Positioning and Power in Academic Publishing: Players, Agents and Agendas; Loizides, F.; Schmidt, B., Eds. IOS Press, 2016, pp. 87 – 90.
40. Lindsay, J. The whitebox geospatial analysis tools project and open-access GIS. Proceedings of the GIS research UK 22nd annual conference, The University of Glasgow, 2014, pp. 16–18.
41. Jordahl, K.; den Bossche, J.V.; Fleischmann, M.; Wasserman, J.; McBride, J.; Gerard, J.; Tratner, J.; Perry, M.; Badaracco, A.G.; Farmer, C.; Hjelle, G.A.; Snow, A.D.; Cochran, M.; Gillies, S.; Culbertson, L.; Bartos, M.; Eubank, N.; maxalbert.; Bilogur, A.; Rey, S.; Ren, C.; Arribas-Bel, D.; Wasser, L.; Wolf, L.J.; Journois, M.; Wilson, J.; Greenhall, A.; Holdgraf, C.; Filipe.; Leblanc, F. geopandas/geopandas: v0.8.1, 2020. doi:10.5281/zenodo.3946761.

42. Hoyer, S.; Hamman, J. xarray: N-D labeled arrays and datasets in Python. *Journal of Open Research Software* **2017**, *5*. doi:10.5334/jors.148.
43. Braun, R. sertit-utils: 1.39.1, 2024.
44. Scown, M.W.; Thoms, M.C.; De Jager, N.R. Floodplain complexity and surface metrics: Influences of scale and geomorphology. *Geomorphology* **2015**, *245*, 102–116. doi:10.1016/j.geomorph.2015.05.024.
45. Etkin, D. Risk transference and related trends: driving forces towards more mega-disasters. *Environmental Hazards* **1999**, *1*, 69–75. doi:10.3763/ehaz.1999.0109.
46. Chini, M.; Pelich, R.; Pulvirenti, L.; Pierdicca, N.; Hostache, R.; Matgen, P. Sentinel-1 InSAR coherence to detect floodwater in urban areas: Houston and Hurricane Harvey as a test case. *Remote Sensing* **2019**, *11*, 107.
47. Gens, R.; Van Genderen, J.L. Review Article SAR interferometry—issues, techniques, applications. *International journal of remote sensing* **1996**, *17*, 1803–1835.

Disclaimer/Publisher’s Note: The statements, opinions and data contained in all publications are solely those of the individual author(s) and contributor(s) and not of MDPI and/or the editor(s). MDPI and/or the editor(s) disclaim responsibility for any injury to people or property resulting from any ideas, methods, instructions or products referred to in the content.